Attosecond streaking with twisted X waves and intense infrared pulses

Birger Böning,[1,*] Willi Paufler,[1] and Stephan Fritzsche[1,2]
[1]*Theoretisch-Physikalisches Institut, Friedrich-Schiller-Universität Jena, 07743 Jena, Germany*
[2]*Helmholtz-Institut Jena, 07743 Jena, Germany*
(Received 25 July 2017; published 26 October 2017)

We investigate the photoionization of atoms by attosecond X waves carrying orbital angular momentum in the presence of a strong, linearly polarized, near infrared (NIR) laser pulse. In the plane-wave case, the streaking of photoelectrons by the NIR pulse has been used to characterize the ionizing pulse. In contrast to plane-wave pulses, X waves have a spatially dependent temporal profile, which modifies the ionization process. Here we explore theoretically the influence of this complex pulse structure on the streaking of photoelectrons for both localized and macroscopically extended targets. On the basis of the strong-field approximation, we find that the streaking spectra of localized targets sensitively depend on the opening angle of the X wave and the position of the atomic target relative to the beam axis. For macroscopically extended targets, we find that the streaking spectra do not depend on the parameters characterizing the twist of the X wave.

DOI: 10.1103/PhysRevA.96.043423

I. INTRODUCTION

Probing electronic dynamics on the attosecond time scale is essential for our understanding of many fundamental processes in matter. In recent years, this dynamics has become accessible due to advances in the generation and control of ultrashort laser pulses [1–3]. Major experimental results based on the interaction of such pulses with electronic systems include the measurement of time delays in photoemission [4] and the dynamics of excited states in noble gases [5], imaging of the charge migration in large molecules [6,7], and the investigation of many-electron effects in solid-state physics [8].

Attosecond pulses can routinely be produced by high-harmonic generation [9] and consist of only a few optical cycles. Utilizing such pulses to probe ultrafast electronic processes crucially relies on their temporal characterization in order to derive meaningful interpretations of time-resolved measurements. Various schemes have been developed to fit this purpose and allow the determination of the duration or even the full time dependence of attosecond pulses [10–13].

A prominent example of such a scheme is the attosecond streak camera [12]. It is based on the photoionization of atoms by an attosecond pulse in the presence of a moderately strong near infrared (NIR) pulse. During the process of ionization, the temporal structure of the attosecond pulse is imprinted on the photoelectron wave packet. The NIR pulse then streaks the photoelectrons away from the ion and acts as an ultrafast phase modulator on this wave packet: If the phase of the dressing field at the time of ionization is varied, the temporal structure of the wave packet is mapped to its energy distribution. This allows the extraction of both pulse duration and chirp from the photoelectron spectra [10].

Besides manipulating the temporal shape of laser pulses, one can tailor their spatial wave form. In particular, twisted light beams with a helical phase structure can be created using, for example, computer-generated holograms [14], spiral phase plates [15], or axicons [16]. These beams carry not only spin angular momentum but also orbital angular momentum. This property promises new ways of manipulating light-matter interactions including the control of trapped microparticles [17,18]. Furthermore, various studies have examined theoretically the modification of photoionization and excitation of atoms due to the twisted nature of the incoming light [19,20]. In both cases the photon angular momentum can be transferred to the electron. Assuming, for example, a single hydrogen atom ionized by a beam carrying l units of orbital angular momentum, one finds that transitions must obey the rules $\Delta L \leqslant |l| + 1$ and $\Delta M = l \pm 1$, where $\Delta L + |l| + 1$ is even [21].

Moreover, recent studies have shown that orbital angular momentum is transferred in the process of high-harmonic generation, which opens the way to the generation of twisted pulses of attosecond duration [22–25]. Methods have also been proposed to generate twisted pulses of high energy for free-electron lasers [26,27].

On the theoretical side, twisted pulses can be described by X waves, which are composed of a superposition of Bessel beams. They have attracted much attention in optics [28,29], condensed-matter physics [30], and optical communications [31]. While most of these works deal with low-order X waves, pulses carrying a higher total angular momentum (TAM) have been introduced recently [32–34]. It was shown that the spatially varying spectral profile of the X waves can be probed by the photoionization of reasonably localized targets [35].

The interaction of atoms and molecules with laser pulses that are tailored in both space and time paves the way for the study of ultrafast processes involving a transfer of orbital angular momentum. However, this requires a proper temporal characterization of twisted pulses in the attosecond domain.

In this work, we therefore investigate the attosecond streaking when the ionizing pulse is an X wave. In Sec. II, the theoretical methods based on the strong-field approximation (SFA) are introduced. We begin our discussion with the transition amplitude for the two-color ionization with X waves and strong NIR pulses in Sec. II A. Based on the transition amplitude, we define the streaking spectra that are measured in an attosecond streaking experiment. In Sec. II B, we introduce X wave pulses and explain their characteristics. We then

*birger.boening@uni-jena.de

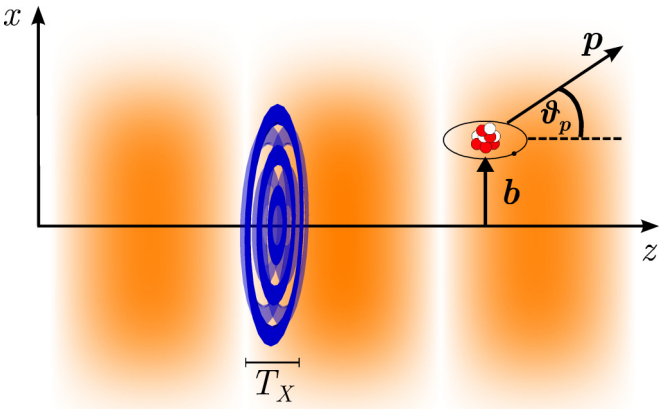

FIG. 1. Setup of the two-color ionization by a short twisted X wave pulse (blue) and a moderately strong NIR field (orange) that is linearly polarized in the x direction. The atomic target is localized at the impact parameter $\boldsymbol{b} = (b,\varphi_b = 0, z_b = 0)$ relative to the beam z axis. The photoelectrons are observed with asymptotic momentum $\boldsymbol{p} = (p,\vartheta_p,\varphi_p)$ at the detector.

explicitly evaluate the transition amplitude in Sec. II C. With the resulting expression, we perform detailed computations of the streaking spectra, which are discussed in Sec. III. Emphasis is placed on the dependence of the streaking spectra on the TAM as well as the opening angle of the X wave pulse. For localized targets, we show that the streaking spectra sensitively depend on the opening angle, while a change in the TAM of the pulse only has a minor effect. We also discuss macroscopically extended targets of infinite size. There we find that the dependence of the streaking spectra on the parameters characterizing the twist of the X wave is lost. Finally, a summary and an outlook are given in Sec. IV.

Note that atomic units ($m_e = e = \hbar = 4\pi\varepsilon_0 = 1$) are used throughout the paper unless stated otherwise.

II. THEORETICAL METHODS

A. Two-color ionization and streaking spectra

The attosecond streaking considered in this work is a two-color ionization process. Figure 1 shows a typical setup for the two-color ionization of atoms by an X wave pulse of duration T_X and a strong NIR pulse with many cycles. We assume that the X wave pulse is short compared to the NIR cycle length. That is, $T_X \ll 2\pi/\omega_L$, where ω_L is the central frequency of the NIR pulse. A single atomic target is placed at impact parameter $\boldsymbol{b} = (b,\varphi_b = 0, z_b = 0)$ relative to the beam axis, which is common to both pulses. Furthermore, we assume that the X wave is energetic enough to ionize the target atom, $\omega_X > E_B$, where ω_X is the X wave's central frequency and $E_B > 0$ is the binding energy of the initial state of the electron.

At a moderate intensity I of the NIR pulse with central frequency $\omega_L \ll E_B$, the NIR pulse does not contribute to the ionization of the atom. However, a photoelectron released from the atom by the X wave pulse will be accelerated by the NIR pulse towards the detectors, where its asymptotic momentum $\boldsymbol{p} = (p,\vartheta_p,\varphi_p)$ is eventually measured. This subsequent acceleration is called streaking of the photoelectron by the NIR pulse. We take the NIR pulse to be polarized in the x direction and assume that the detectors are aligned in this direction. That is, we set $\vartheta_p = \pi/2$ and $\varphi_p = 0$.

In order to describe the two-color ionization theoretically, we consider a single-active electron, which is bound in the target atom in a hydrogenlike $1s$ state $|\Psi_0(t)\rangle = |\Phi_0\rangle e^{iE_B t}$. Our aim is to compute the amplitude for the transition of this active electron from the bound state to the continuum dressed by the NIR laser pulse. In the SFA, the continuum states are given by Volkov wave functions $|\Psi_{\boldsymbol{p}}^{(V)}(t)\rangle = |\boldsymbol{q}(t)\rangle e^{-iS_V(t)}$, where $\boldsymbol{q}(t) = \boldsymbol{p} + \boldsymbol{A}_L(t)$ is the electron's canonical momentum and the Volkov phase is given by

$$S_V(t) = \frac{1}{2}\int^t dt'[\boldsymbol{p} + \boldsymbol{A}_L(t')]^2. \tag{1}$$

Here $\boldsymbol{A}_L(t)$ is the vector potential of the NIR pulse. We employ the length gauge for $\boldsymbol{A}_L(t)$ so that $\boldsymbol{p}$ is the physical momentum of the photoelectron [36]. Since we assume a many-cycle NIR laser pulse, we write its vector potential simply as a plane wave of the form

$$\boldsymbol{A}_L(t) = A_{L0}\cos(\omega_L t + \phi_L)\boldsymbol{e}_x. \tag{2}$$

For the vector potential $\boldsymbol{A}_X(\boldsymbol{r},t)$ of the X wave, however, we use the velocity gauge because of its dependence on the spatial coordinates $\boldsymbol{r}$.

With these assumptions in mind, the transition amplitude for the two-color ionization is given by [37]

$$\mathcal{T}_{\boldsymbol{b}}(\boldsymbol{p},\phi_L) = -i\int_{-\infty}^{\infty} dt\,\langle\Psi_{\boldsymbol{p}}^{(V)}(t)|\,\hat{\boldsymbol{p}}\cdot\boldsymbol{A}_X(\boldsymbol{r},t)\,|\Psi_0(t)\rangle, \tag{3}$$

where we treat the interaction between the electron and the X wave pulse in first-order time-dependent perturbation theory. This is valid, since we assume a weak X wave pulse with central frequency $\omega_X > E_B$. Equation (3) explicitly indicates the dependence of the transition amplitude on the impact parameter of the target and the phase of the NIR field.

With the two-color transition amplitude (3), we can compute the energy- and angle-differential photoionization probability for the two-color ionization of a single atom at the impact parameter **b**,

$$\mathbb{P}_{\boldsymbol{b}}(\boldsymbol{p},\phi_L) = |\mathcal{T}_{\boldsymbol{b}}(\boldsymbol{p},\phi_L)|^2. \tag{4}$$

We assume that the ionizing X wave pulse is centered around $t = 0$. Therefore, the relative phase ϕ_L of the NIR field (2) defines a time delay τ between the maximum of the X wave pulse and the first maximum of the NIR field,

$$\phi_L(\tau) = \omega_L\tau. \tag{5}$$

In a typical streaking experiment, the two-color ionization probability (4) is measured as function of the photoelectron energy E_p and the time delay τ between the two pulses,

$$\mathbb{P}_{\boldsymbol{b}}(E_p,\tau) = |\mathcal{T}_{\boldsymbol{b}}(\boldsymbol{p}(E_p),\phi_L(\tau))|^2, \tag{6}$$

where $\boldsymbol{p}(E_p) = (\sqrt{2E_p},\vartheta_p = \pi/2,\varphi_p = 0)$. The photoionization probability (6), parametrized by E_p and τ, is also called the streaking spectrum.

In Sec. III, we will analyze the dependence of the streaking spectrum on the properties of the ionizing X wave pulse.

Before doing so, we first need to introduce X waves and evaluate the transition amplitude (3).

B. Characterization of X waves

X waves are nondiffracting pulses carrying orbital angular momentum, which are formed by a superposition of Bessel beams. These Bessel beams $\boldsymbol{A}_{m\Lambda\vartheta_k}(\boldsymbol{r},t)$ are solutions of the wave equation

$$\left(\triangle - \alpha^2 \frac{\partial^2}{\partial t^2}\right)\boldsymbol{A}_{m\Lambda\vartheta_k}(\boldsymbol{r},t) = 0 \tag{7}$$

and are characterized by the helicity Λ, the cone opening angle ϑ_k in momentum space, and the projection m of TAM onto their beam axis,

$$\hat{J}_z \boldsymbol{A}_{m\Lambda\vartheta_k}(\boldsymbol{r},t) = m\boldsymbol{A}_{m\Lambda\vartheta_k}(\boldsymbol{r},t), \tag{8}$$

where $\hat{J}_z = \hat{L}_z + \hat{S}_z$ is the operator of TAM projection with the operators $\hat{L}_z$ of orbital angular momentum projection and $\hat{S}_z$ of spin projection. We note that the solutions to (7) and (8) constructed in the following do not carry a definite orbital angular momentum. However, Bessel beams have a well-defined TAM due to Eq. (8). Therefore, we will use the TAM m when specifying the angular momentum of the beam. Only in the paraxial limit are orbital and spin angular momenta separately defined (see the end of this section).

The vector potential of a Bessel beam in the Coulomb gauge can be represented by a superposition of circularly polarized plane waves with helicity Λ [19],

$$\boldsymbol{A}_{m\Lambda\vartheta_k}(\boldsymbol{r},t) = \int \frac{d^2\boldsymbol{k}_\perp}{(2\pi)^2} a_{\varkappa m}(\boldsymbol{k}_\perp) e^{i(\boldsymbol{k}\boldsymbol{r}-\omega t)} \boldsymbol{\varepsilon}_{\boldsymbol{k}\Lambda}, \tag{9}$$

with wave vectors $\boldsymbol{k} = (\boldsymbol{k}_\perp, k_z) = (\varkappa, \varphi_k, k_z)$. Here the opening angle $\vartheta_k = \arctan(\varkappa/k_z)$ relates transversal ($\varkappa$) and longitudinal (k_z) momenta. In Eq. (9), the expansion coefficients read

$$a_{\varkappa m}(\boldsymbol{k}_\perp) = (-1)^m \sqrt{\frac{2\pi}{k_\perp}} e^{im\varphi_k} \delta(k_\perp - \varkappa). \tag{10}$$

The polarization vectors $\boldsymbol{\varepsilon}_{\boldsymbol{k}\Lambda}$ of the plane-wave components depend on the helicity Λ and the wave vector $\boldsymbol{k}$ and are given by

$$\boldsymbol{\varepsilon}_{\boldsymbol{k}\lambda} = -\frac{\Lambda}{\sqrt{2}} \begin{pmatrix} \cos\vartheta_k \cos\varphi_k - i\Lambda \sin\varphi_k \\ \cos\vartheta_k \sin\varphi_k + i\Lambda \cos\varphi_k \\ -\sin\vartheta_k \end{pmatrix}. \tag{11}$$

In order to describe the interaction of atoms with twisted light on a short time scale, we need to construct a twisted pulse of finite duration T_X. Experimentally, such pulses can be created as nonmonochromatic superpositions of continuous Bessel beams [38]. Such a superposition can mathematically be described by convoluting the monochromatic Bessel solution (9) with a Gaussian spectral distribution of width $\Delta\omega = 1/T_X$ while keeping the opening angle ϑ_k fixed. This results in the X wave vector potential

$$\boldsymbol{A}_X(\boldsymbol{r},t) = \int_0^\infty \frac{d\omega}{\sqrt{2\pi}\Delta\omega} \exp\left[-\frac{1}{2}\left(\frac{\omega-\omega_0}{\Delta\omega}\right)^2\right] \boldsymbol{A}_{m\Lambda\vartheta_k}(\boldsymbol{r},t), \tag{12}$$

which is characterized by the quantum numbers Λ, m, and ϑ_k as defined above as well as the central frequency ω_0 and the pulse duration T_X.

For later analysis of the streaking spectra, it is instructive to examine the plane-wave limit of Eq. (12). To do so, we first write the Bessel beam (9) in a spin basis

$$\boldsymbol{A}_{m\Lambda\vartheta_k}(\boldsymbol{r},t) = e^{-i\omega t} \sum_{m_s=0,\pm1} \boldsymbol{\eta}_{m_s} A^{\mathrm{tw}}_{m_s}(\boldsymbol{r}), \tag{13}$$

where $\boldsymbol{\eta}_{m_s}$ ($m_s = 0, \pm 1$) are eigenvectors of the spin projection operator $\hat{S}_z$,

$$\hat{S}_z \boldsymbol{\eta}_{m_s} = m_s \boldsymbol{\eta}_{m_s}, \quad \boldsymbol{\eta}_0 = \begin{pmatrix} 0 \\ 0 \\ 1 \end{pmatrix}, \quad \boldsymbol{\eta}_{\pm1} = \frac{\mp1}{\sqrt{2}} \begin{pmatrix} 1 \\ \pm i \\ 0 \end{pmatrix}, \tag{14}$$

and the coefficients $A^{\mathrm{tw}}_{m_s}(\boldsymbol{r})$ are given by

$$A^{\mathrm{tw}}_{m_s}(\boldsymbol{r}) = \sqrt{\frac{\varkappa}{2\pi}} (-i)^{m_s} c_{m_s} J_{m-m_s}(\varkappa r) e^{i(m-m_s)\varphi_r} e^{ik_z z}. \tag{15}$$

Here $J_{m-m_s}(\varkappa r)$ are Bessel functions of the first kind. From Eq. (15) we can deduce the paraxial limit ($\vartheta_k \ll 1$) of the Bessel beam. In this limit, the coefficients

$$c_{\pm1} = \frac{1}{2}(1 \pm \cos\vartheta_k), \quad c_0 = \frac{\Lambda}{\sqrt{2}} \sin\vartheta_k \tag{16}$$

imply that only the term $m_s = \Lambda$ remains in the summation in Eq. (13),

$$\boldsymbol{A}^{\mathrm{p}}(\boldsymbol{r},t) = \boldsymbol{\eta}_\Lambda \sqrt{\frac{\varkappa}{2\pi}} (-i)^\Lambda c_\Lambda J_{m-\Lambda}(\varkappa r) e^{i(m-\Lambda)\varphi_r} e^{i(k_z z - \omega t)}. \tag{17}$$

It can be easily checked that the projections of spin and orbital angular momenta of $\boldsymbol{A}^{\mathrm{p}}(\boldsymbol{r},t)$ decouple in this limit,

$$\hat{S}_z \boldsymbol{A}^{\mathrm{p}}(\boldsymbol{r},t) = \Lambda \boldsymbol{A}^{\mathrm{p}}(\boldsymbol{r},t), \tag{18}$$

$$\hat{L}_z \boldsymbol{A}^{\mathrm{p}}(\boldsymbol{r},t) = (m-\Lambda)\boldsymbol{A}^{\mathrm{p}}(\boldsymbol{r},t). \tag{19}$$

Moreover, in this limit $\varkappa = k \sin\vartheta \to 0$, which implies $J_{m-\Lambda}(\varkappa r) \to \delta_{m\Lambda}$. Thus, Eq. (17) approaches a standard plane-wave solution and the X wave vector potential (12) reduces to a circularly polarized plane-wave pulse in the paraxial limit.

C. Evaluation of transition amplitude

We now turn to the analysis of the two-color transition amplitude (3). Due to the spatial dependence of the X wave vector potential (12), the transition amplitude also depends on the location of the target atom relative to the beam axis, that is, on the impact parameter $\boldsymbol{b} = (b, \varphi_b = 0, b_z = 0)$. Using Eq. (12), the transition amplitude (3) becomes a superposition of transition amplitudes $\mathcal{T}^{(\mathrm{tw})}_{\omega\boldsymbol{b}}(\boldsymbol{p},\phi_L)$ for monochromatic Bessel beams,

$$\mathcal{T}_{\boldsymbol{b}}(\boldsymbol{p},\phi_L) = \int_0^\infty \frac{d\omega}{\sqrt{2\pi}\Delta\omega} \exp\left[-\frac{1}{2}\left(\frac{\omega-\omega_0}{\Delta\omega}\right)^2\right] \times \mathcal{T}^{(\mathrm{tw})}_{\omega\boldsymbol{b}}(\boldsymbol{p},\phi_L), \tag{20}$$

each of which can in turn be written as

$$\mathcal{T}^{(\mathrm{tw})}_{\omega \boldsymbol{b}}(\boldsymbol{p},\phi_L) = \int \frac{d^2\boldsymbol{k}_\perp}{(2\pi)^2} a_{\varkappa m}(\boldsymbol{k}_\perp) e^{i\boldsymbol{k}\boldsymbol{b}} \mathcal{T}^{(\mathrm{pw})}(\boldsymbol{p},\boldsymbol{k},\phi_L). \quad (21)$$

Here $\mathcal{T}^{(\mathrm{pw})}(\boldsymbol{p},\boldsymbol{k},\phi_L)$ are the typical plane-wave transition amplitudes

$$\mathcal{T}^{(\mathrm{pw})}(\boldsymbol{p},\boldsymbol{k},\phi_L) = -i \int_{-\infty}^{\infty} dt\, \boldsymbol{q}(t) \cdot \boldsymbol{\varepsilon}_{\boldsymbol{k}\Lambda} \langle \boldsymbol{q}(t)|\, e^{i\boldsymbol{k}\boldsymbol{r}}\, |\Phi_0\rangle e^{i(E_B-\omega)t + iS_V(t)} \quad (22)$$

that occur also in the analysis of the two-color ionization with plane-wave pulses [39]. In order to perform the time integration in Eq. (22), we need to evaluate the Volkov phase (1) for the linearly polarized NIR field (2). This yields the Volkov phase factor

$$e^{iS_V(t)} = e^{i(p^2/2+U_p)t} \sum_{n_1,n_2=-\infty}^{\infty} J_{n_1}(\alpha_L) J_{n_2}(\beta_L) \times e^{i(n_1+2n_2)\omega_L t} e^{i(n_1+2n_2)\phi_L}, \quad (23)$$

if one applies the Jacobi-Anger expansion [40] and makes use of the so-called ponderomotive potential $U_p = A_{L0}^2/4$ and where the coefficients are given by $\alpha_L = (A_{L0} p \sin\vartheta_p \cos\varphi_p)/\omega_L$ and $\beta_L = A_{L0}^2/8\omega_L$.

If we use, in addition, the explicit form (11) of the polarization vector, we can evaluate the scalar product in Eq. (22),

$$\begin{aligned}\boldsymbol{q}(t) \cdot \boldsymbol{\varepsilon}_{\boldsymbol{k}\boldsymbol{\Lambda}} = -\frac{\Lambda_X}{\sqrt{2}} \{ & p[\sin\vartheta_p \cos\vartheta_k \cos(\varphi_k - \varphi_p) \\ & - \cos\vartheta_p \sin\vartheta_k - i\Lambda \sin\vartheta_p \sin(\varphi_k - \varphi_p)] \\ & + A_{L0} \cos(\omega_L t + \phi_L)(\cos\vartheta_k \cos\varphi_k - i\Lambda \sin\varphi_k)\}. \end{aligned} \quad (24)$$

With Eqs. (23) and (24), the plane-wave amplitudes (22) become

$$\begin{aligned}\mathcal{T}^{(\mathrm{pw})}(\boldsymbol{p},\boldsymbol{k},\phi_L) = -i \sum_{n_1,n_2=-\infty}^{\infty} & F_{n_1 n_2}(\vartheta_k,\varphi_k) e^{i(n_1+2n_2)\phi_L} \\ & \times \int_{-\infty}^{\infty} dt \langle \boldsymbol{q}(t)|\, e^{i\boldsymbol{k}\boldsymbol{r}}\, |\Phi_0\rangle \exp\left[i\left(\frac{p^2}{2} \right.\right. \\ & \left.\left. + U_p + E_B - \omega + (n_1+2n_2)\omega_L \right) t \right], \end{aligned} \quad (25a)$$

$$\begin{aligned} F_{n_1 n_2}(\vartheta_k,\varphi_k) = -\frac{\Lambda_X}{\sqrt{2}} J_{n_1}(\alpha_L) J_{n_2}(\beta_L) \Big[& p \sin\vartheta_p [\cos\vartheta_k \\ & \times \cos(\varphi_k - \varphi_p) - i\Lambda_X \sin(\varphi_k - \varphi_p)] \\ & - p \cos\vartheta_p \sin\vartheta_k + \frac{n_1 A_{L0}}{\alpha_L} (\cos\vartheta_k \cos\varphi_k \\ & - i\Lambda_X \sin\varphi_k) \Big]. \end{aligned} \quad (25b)$$

No approximations have been made so far to obtain Eqs. (25). In general, however, the time integration in Eq. (25a) is not easy to perform explicitly. We can further simplify the integrand in this time integral if we assume a sufficiently weak NIR field when compared to the asymptotic momentum of the electron, $A_{L0} \ll p$. This allows us to approximate $\boldsymbol{q}(t) \approx \boldsymbol{p}$, which eventually leads to a time-independent matrix element in Eq. (25a). For a sufficiently weak NIR field, we can therefore perform the time integration in Eq. (25a),

$$\int_{-\infty}^{\infty} dt\, e^{i[p^2/2 + U_p + E_B - \omega + (n_1+2n_2)\omega_L]t} = 2\pi\delta(\omega_{n_1 n_2}(p) - \omega), \quad (26)$$

where $\omega_{n_1 n_2}(p) = \frac{p^2}{2} + U_p + E_B + (n_1+2n_2)\omega_L$.

Using the properties of the δ function, we can use the result (26) to carry out the ω integration in the two-color transition amplitude (20). However, this transition amplitude still contains an integral over the transverse momenta of the plane-wave components resulting from Eq. (21). To further simplify this integral, we make use of the dipole approximation in the matrix element

$$\langle \boldsymbol{p}|\, e^{i\boldsymbol{k}\boldsymbol{r}}\, |\Phi_0\rangle \approx \langle \boldsymbol{p}|\Phi_0\rangle, \quad (27)$$

which is valid as long as the target is not close to the beam axis, where the X wave has a phase singularity.

With these simplifications, we can finally write the two-color transition amplitude for an atom placed at impact parameter $\boldsymbol{b}$ as

$$\begin{aligned}\mathcal{T}_{\boldsymbol{b}}(\boldsymbol{p},\phi_L) = -i \frac{(2\pi)^{3/2}}{\Delta\omega} \langle \boldsymbol{p}|\Phi_0\rangle & \\ \times \sum_{n_1,n_2=-\infty}^{\infty} I_{n_1 n_2}(\boldsymbol{b}) \exp\left[-\frac{1}{2} \left(\frac{\omega_{n_1 n_2}(p) - \omega_0}{\Delta\omega} \right)^2 \right] & \\ \times e^{i(n_1+2n_2)\phi_L}, & \end{aligned} \quad (28)$$

where the coefficients in the double summation are given by

$$I_{n_1 n_2}(\boldsymbol{b}) = \int \frac{d^2\boldsymbol{k}_\perp}{(2\pi)^2} a_{\varkappa m}(\boldsymbol{k}_\perp) e^{i\boldsymbol{k}\boldsymbol{b}} F_{n_1 n_2}(\vartheta_k,\varphi_k). \quad (29)$$

In order to compute numerical values for the transition amplitude, these integrals can be evaluated analytically using Eqs. (10) and (25b) and the integral representation of the Bessel functions.

In our computations of the streaking spectra (6) below, we restricted the (infinite) double summation in the transition amplitude (28) to the finite values $-14 \leqslant n_1 \leqslant 14$ and $-4 \leqslant n_2 \leqslant 4$. This restriction still yields accurate results, since the contributions of higher terms decrease exponentially due to $\omega_{n_1 n_2}(p)$ in the exponent in Eq. (28).

Let us note that in the limit of a long X wave pulse with duration $T_X \gg 2\pi/\omega_L$, the infinite double summation over n_1 and n_2 in Eq. (28) gives rise to the so-called sidebands in the photoelectron spectra. Such a two-color photoionization with a continuous Bessel beam and in the presence of a NIR field was explored recently in [37].

III. RESULTS AND DISCUSSION

In the preceding section, we derived an expression for the transition amplitude for a localized target. As seen from the final result (28), the streaking spectrum (6) depends on

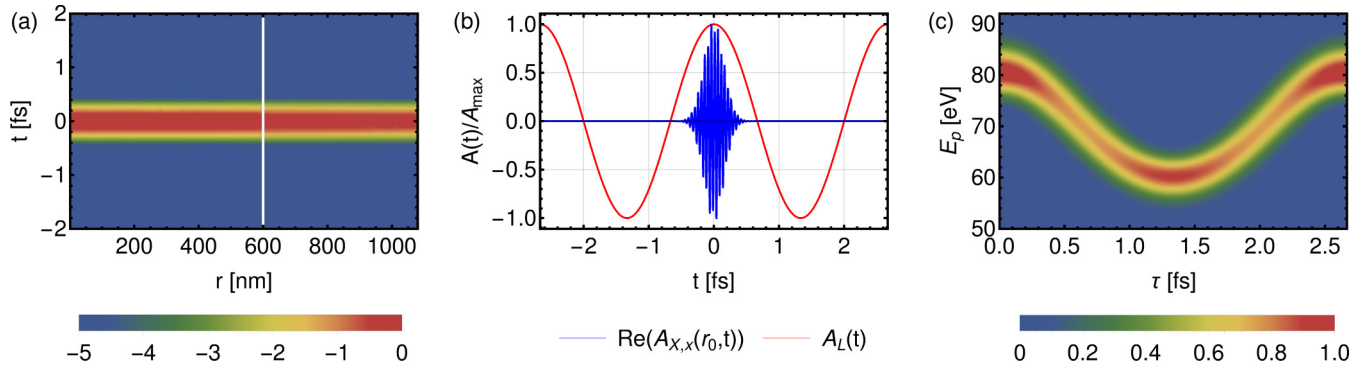

FIG. 2. Streaking of photoelectrons in a continuous NIR field following the ionization by a short X wave pulse in the plane-wave limit $\vartheta_k \ll 1$, $m = \Lambda$. (a) Modulus of the X wave vector potential as a function of the distance r from the beam axis and time t on a logarithmic scale. (b) Real part of the x component $A_{X,x}(r_0 = 600\text{ nm},t)$ of the X wave pulse (blue) and the NIR field (red) as functions of time for time delay $\tau = 0$. (c) Streaking spectrum $\mathbb{P}_{\boldsymbol{b}}(E_p,\tau)$ for a single-atom target with binding energy $E_B = 11.7$ eV and at impact parameter $b = 600$ nm. All quantities are normalized to their respective maxima. Results are shown for an X wave with $T_X = 150$ as, $\vartheta_k = 10^{-3\circ}$, $\Lambda = +1$, $\omega_X = 81.6$ eV, and a NIR field with $\lambda = 800$ nm and $I = 3.5\times10^{12}$ W/cm^2.

NIR laser parameters, X wave parameters, and the binding energy of the initial state. We now aim to understand how the TAM projection m and the opening angle ϑ_k of the X wave pulse affect the streaking spectra. In the computation of the streaking spectra below, we set the NIR wavelength and intensity equal to $\lambda = 800$ nm and $I = 3.5\times10^{12}$ W/cm^2 ($A_{L0} \approx 0.18$ a.u.), respectively. Moreover, we assume a target with binding energy $E_B = 11.7$ eV (for example, Ca^+) at $\boldsymbol{b} = (b,\varphi_b = 0,b_z = 0)$ and consider an X wave with central energy $\omega_X = 81.6$ eV, pulse duration $T_X = 150$ as, and helicity $\Lambda = +1$.

A. Plane-wave limit

Let us first consider streaking spectra from an X wave pulse in the plane-wave limit. As discussed above in Sec. II B, X waves coincide with a plane-wave for $\vartheta_k \ll 1$ and $m = \Lambda$. In Fig. 2(a), the modulus of the resulting vector potential is shown as a function of time t and distance r from the beam axis. Independently of the radial coordinate, the vector potential exhibits a single maximum in time that describes a single circularly polarized XUV pulse of FWHM duration T_X. To compute the photoionization probability, we place the atomic target at $b = 600$ nm. Note that, at this point, the choice of impact parameter is not important, since the plane-wave limit of the X wave is independent of r. Figure 2(b) shows the real part of the x component of the XUV pulse (blue) at this impact parameter together with the NIR field (red) for a time delay $\tau = 0$. In the ionization process, the electron leaves the atom at time $t_i = 0$. From conservation of canonical momentum, the final photoelectron momentum at the detector is given by

$$\begin{aligned}\boldsymbol{p}_f &= \boldsymbol{p}_i + \boldsymbol{A}_L(t_i)\\ &= \boldsymbol{p}_i + A_{L0}\cos[\omega_L t_i + \phi_L(\tau)]\boldsymbol{e}_x\\ &= \boldsymbol{p}_i + A_{L0}\cos[\omega_L(t_i+\tau)]\boldsymbol{e}_x,\end{aligned} \tag{30}$$

where $\boldsymbol{p}_i$ is the momentum at time of ionization and we made use of Eq. (5). In streaking measurements, the photoelectron momentum is measured as a function of τ. From Eq. (30) we see that this reproduces a trace of the NIR field in the streaking spectrum.

However, the ionization time t_i is not sharply defined. Instead, the finite duration T_X of the ionizing pulse imposes an uncertainty on t_i. The streaking spectrum, shown in Fig. 2(c), therefore exhibits a broadened image of the NIR field, where the broadening in energy depends on T_X. From a measurement of this spectrum, one can directly read off the cycle length ($\sim$2.7 fs) of the NIR field and extract the duration of the ionizing pulse. This is discussed, for example, in [10].

B. X waves: Localized targets

Let us now examine the streaking spectra from an X wave of arbitrary opening angle ϑ_k and TAM projection m. In the following, we study the influence of these parameters on the photoionization process in the presence of the NIR field. Thereby, we hold all other parameters fixed as already mentioned in the beginning of the section.

In Fig. 3, the X wave vector potential is visualized as a function of r and t, similar to Fig. 2(a) for the plane-wave limit. More precisely, the modulus of $\boldsymbol{A}_X(\boldsymbol{r},t)$ is displayed for three values of ϑ_k and m. In this figure, we can observe a strong dependence of the temporal shape of the X wave on ϑ_k and m: Rather than consisting of a single pulse independent of position [cf. Fig. 2(a)], it splits into two pulses with increasing opening angle. The temporal separation between these pulses depends on r and the opening angle ϑ_k. An increase in the TAM projection m shifts the first maximum of the X wave away from the beam axis to larger r. Mathematically, this behavior arises from the radial dependence of the Bessel functions in the definition of the X wave [see Eq. (15)].

With this general structure of the X wave vector potential in mind, we now turn to the analysis of the streaking process. The atomic target is placed at the fixed impact parameter $b = 600$ nm (white vertical lines in Fig. 3). Figure 4 shows the streaking spectra as calculated from Eq. (6) for the same X wave parameters as in Fig. 3.

A rather small opening angle of $\vartheta_k = 5^\circ$ yields streaking spectra similar to those found in the plane-wave limit: They exhibit one dominant streaking trace independently of the TAM projection m. However, for $m = 1$ this trace is shifted to higher energies and we see a second trace in the spectrum.

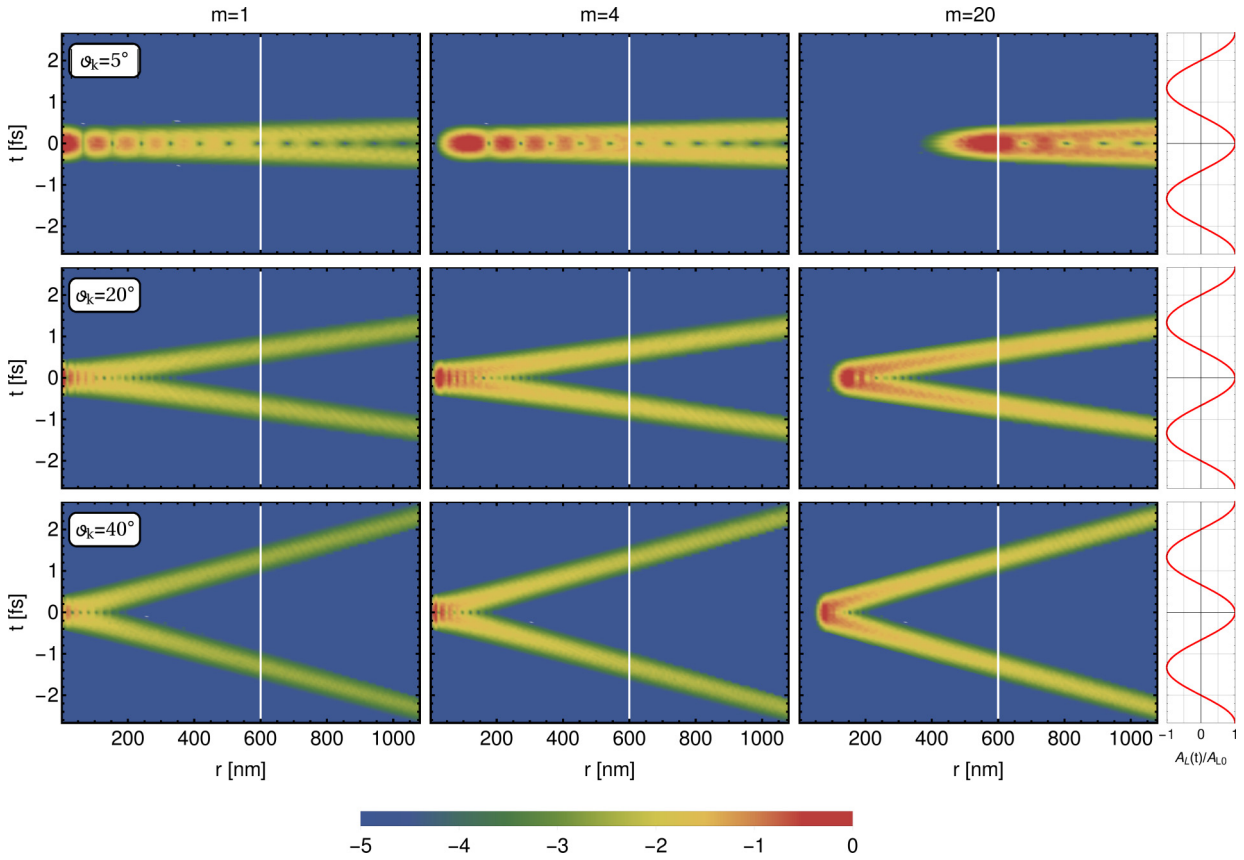

FIG. 3. Vector potential (12) of the X wave pulse as experienced by an atom at $\boldsymbol{r} = (r,\varphi = 0,z = 0)$. The individual plots show the modulus of $\boldsymbol{A}_X(\boldsymbol{r},t)$ as a function of the distance r to the beam axis and time t for three values of the TAM projection m (left column, $m = 1$; center column, $m = 4$; right column, $m = 20$) and three values of the opening angle ϑ_k (top row, $\vartheta_k = 5°$; center row, $\vartheta_k = 20°$; bottom row, $\vartheta_k = 40°$) of the X wave pulse on a logarithmic scale. The modulus is normalized to its maximum in each plot. The rightmost panel shows the NIR field as a function of time for time delay $\tau = 0$. All other parameters are the same as in Fig. 2.

This can be explained by comparison with Fig. 3: The vector potential has two maxima as a function of time t for $\vartheta_k = 5°$ and $m = 1$ at $r = 600$ nm. Therefore, two ionization events take place and release the photoelectron at two different phases of the NIR field. The interferences of these two events are seen in the streaking spectrum. In contrast, for $m = 4$ and 20, the vector potential has only one maximum in time at $r = 600$ nm. No interferences are therefore seen in the corresponding streaking spectra.

For a larger opening angle of $\vartheta_k = 20°$, the dependence of the streaking spectra on the TAM projection is even less pronounced. For $m = 1$, 4, and 20, we see two streaking traces merging in interferences around $\tau = 0$, $T_{\mathrm{IR}}/2$, and T_{IR}. The origin of these interferences is the fact that the vector potential at $b = 600$ nm consists of two pulses separated in time by $T_{\mathrm{IR}}/2$ (see Fig. 3). The two ionization events release the photoelectron into the NIR field at phases ϕ_{L0} and $\phi_{L0} + \pi$, leading to two traces of its vector potential in the streaking spectrum. Interferences between these ionization events occur if the NIR vector potential vanishes for ϕ_{L0}. From Fig. 3 we see that an increase in m does not significantly change the temporal separation of the two pulses defined by $\boldsymbol{A}_X$ at $b = 600$ nm. Therefore, the overall structure of the streaking spectra is not modified by a variation of m. However, the interference structures at $\tau = 0$, $T_{\mathrm{IR}}/2$, and T_{IR} change with m. This reflects the fact that the specific shape of $\boldsymbol{A}_X$ is altered by a change of m due to the shift of the vector potential to larger r (see Fig. 3).

A further increase of the opening angle again strongly modifies the streaking spectra. For $\vartheta_k = 40°$, Fig. 4 displays interferences in the streaking spectra over the full range of τ. Furthermore, the streaking is independent by the TAM projection. The comparison with Fig. 3 reveals that at $b = 600$ nm, $\boldsymbol{A}_X$ consists of two pulses separated by T_{IR}. Therefore, the two ionization events release the photoelectron into the same phase of the NIR field independent of τ, leading to the interferences in the streaking spectra. Furthermore, we see a flip of the streaking trace compared to the plane-wave limit. This arises due to the fact that the X wave's maxima occur at $t = \pm T_{IR}/2$, inducing an overall phase shift of π.

For all other values of the opening angle ϑ_k, which fall in the range between the three values $\vartheta_k = 5°,20°,40°$ discussed above, the streaking spectra will show more complex patterns. These patterns are determined by the temporal separation of the two maxima in the X wave vector potential. For this reason, a variation of the impact parameter has the same effect on the streaking process as a variation of the opening angle. In the following, we therefore vary the impact parameter of the atomic target while keeping the opening angle unchanged. Figure 5 displays the streaking spectra computed at $b = 300$,

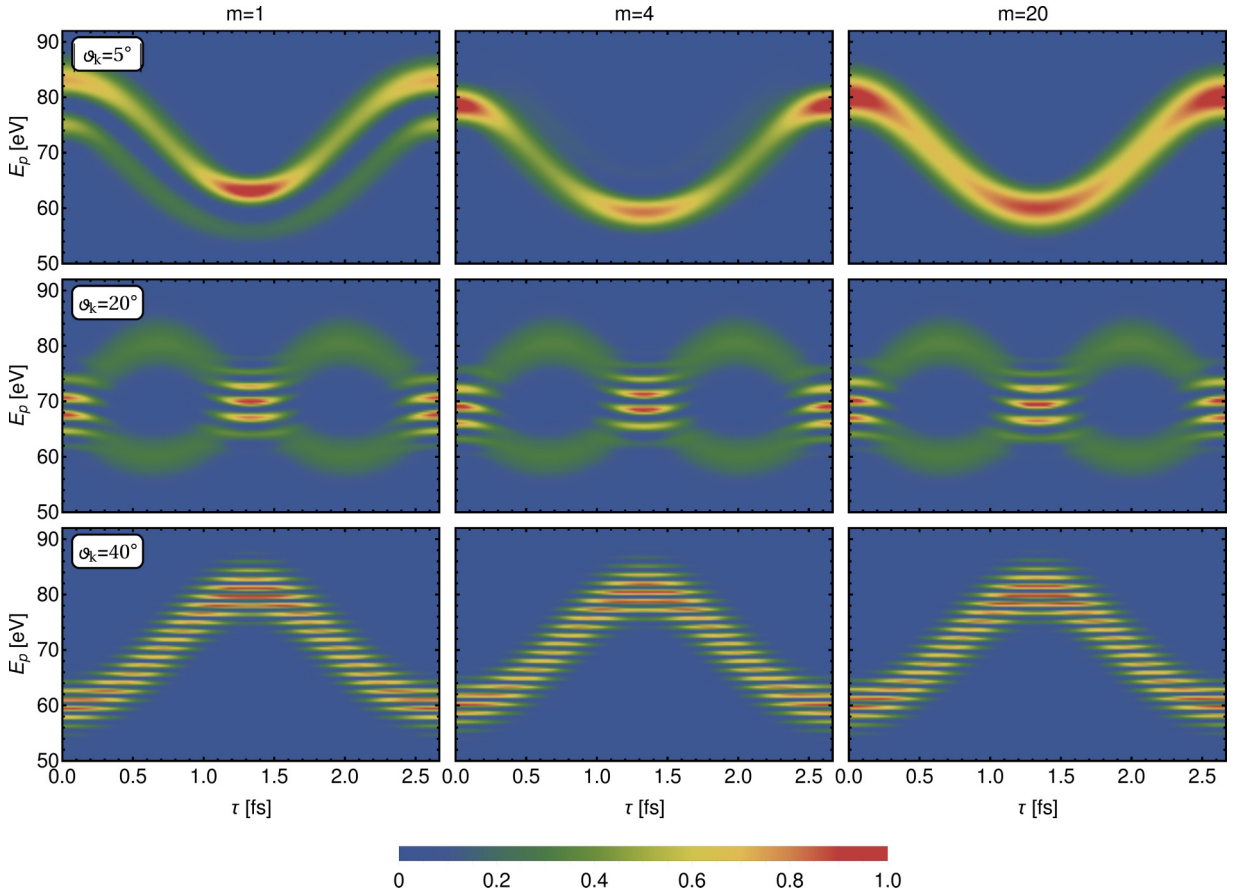

FIG. 4. Streaking of photoelectrons in a continuous NIR field following the ionization by a short X wave pulse. The individual plots show the streaking spectra $\mathbb{P}_b(E_p,\tau)$ for a single-atom target with binding energy $E_B = 11.7$ eV and at impact parameter $b = 600$ nm, but with otherwise the same parameters as in Fig. 3.

600, and 900 nm for the same values of the opening angle as discussed above and $m = 4$. Hence, the central column ($b = 600$ nm) is identical to the second row of Fig. 4. For smaller or larger impact parameters, the streaking spectra show different structures. There, the ionization events are not spaced by integer multiples of $T_{\mathrm{IR}}/2$.

A single trace of $\boldsymbol{A}_L(\tau)$ can still be observed for $\vartheta_k = 5^\circ$ at $b = 300$ nm. However, for $b = 900$ nm, two traces are present, reflecting the fact that the vector potential $\boldsymbol{A}_X$ at $r = 900$ nm consists of two pulses closely separated in time (see Fig. 3). The same behavior is found for $\vartheta_k = 20^\circ$ at $b = 300$ nm. At $b = 900$ nm, the temporal separation of the two pulses almost equals T_{IR} (see Fig. 3), which leads to interferences for all values of τ. If the impact parameter were increased further, this streaking spectrum would transform into the one already discussed for $\vartheta_k = 40^\circ$ and $m = 4$ at $b = 600$ nm. In the third row of Fig. 5, the streaking spectrum shown for $\vartheta_k = 40^\circ$ at $b = 300$ nm is identical to that computed for $\vartheta_k = 20^\circ$ at $b = 600$ nm. This can be expected, since the pulse separation in the X wave vector potential increases linearly with r for a given opening angle, so that we find $T_{\mathrm{IR}}/2$ in this case. For $b = 900$ nm, the pulse separation is $3T_{\mathrm{IR}}/2$, producing again two traces of the NIR vector potential that interfere at $\tau = 0$, $T_{\mathrm{IR}}/2$, and T_{IR}.

The streaking spectra presented so far fall into four categories, which are determined by the structure of the X wave vector potential as presented in Fig. 3: A single pulse (small ϑ_k or small b) in time leads to a single streaking trace of the NIR vector potential, while a split into two pulses leads to two interfering traces (pulse separation is an odd multiple of $T_{\mathrm{IR}}/2$), interferences over the whole range of τ (pulse separation is a multiple of T_{IR}), or transitions between these cases (pulse separation is not an integer multiple of $T_{\mathrm{IR}}/2$).

Since the pulse separation in the X wave vector potential is mainly determined by ϑ_k and b, the streaking process for localized targets depends most strongly on these two parameters. However, as can be seen from Fig. 3, the shift to higher radii induced by an increase of m also leads to a change in the pulse separation. A streaking experiment with an X wave carrying very large TAM will therefore also show a modification of the streaking spectra compared to small m.

The above results demonstrate that the streaking from localized atomic targets leads to complex structures in the photoelectron spectra that reflect the local temporal structure of the ionizing attosecond X wave. Since this local structure is mainly determined by the opening angle of the beam, the streaking spectra show a strong dependence on this parameter.

C. X wave: Extended targets

For actual streaking experiments with X waves, an important question is whether the results found above for localized

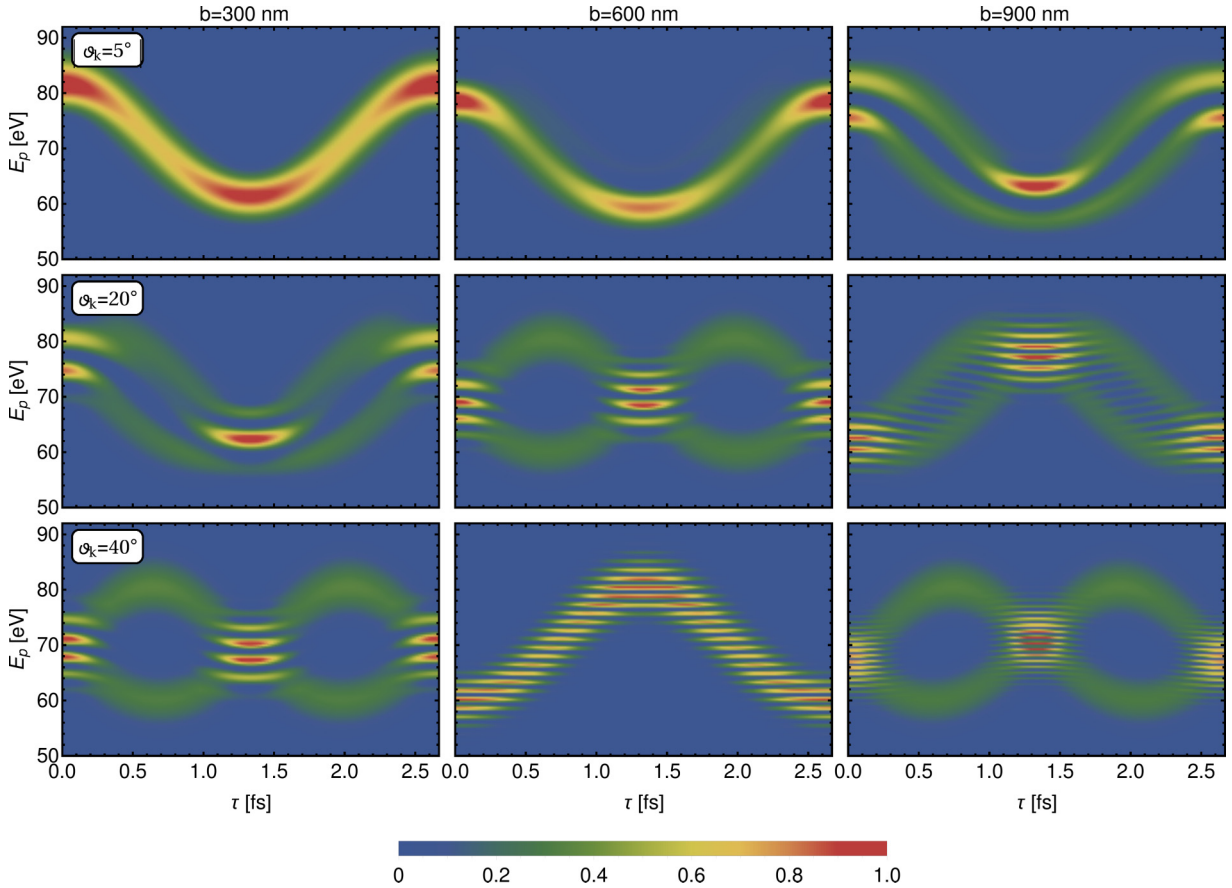

FIG. 5. Same as Fig. 4 but for three different values of the impact parameter b of the target (left column, $b = 300$ nm; center column, $b = 600$ nm; right column, $b = 900$ nm) and three values of the opening angle (top row, $\vartheta_k = 5^\circ$; center row, $\vartheta_k = 20^\circ$; bottom row, $\vartheta_k = 40^\circ$). The TAM projection of the X wave pulse is $m = 4$.

targets also apply to extended targets. To analyze the streaking with macroscopic targets, we assume a homogeneous and (over the cross section of the X wave) infinitely extended target of atoms. To obtain the streaking spectrum for such a target, we incoherently sum the streaking spectra (6) for single-atom targets over all impact parameters

$$\mathbb{P}(E_p,\tau) = \int d^2\boldsymbol{b}\, \mathbb{P}_{\boldsymbol{b}}(E_p,\tau) = \int d^2\boldsymbol{b}\, \mathcal{T}_{\boldsymbol{b}}^*(\boldsymbol{p}(E_p),\phi_L(\tau))\mathcal{T}_{\boldsymbol{b}}(\boldsymbol{p}(E_p),\phi_L(\tau)). \quad (31)$$

The integrations over $\boldsymbol{b}$ and the transverse wave vector $\boldsymbol{k}_\perp$ resulting from Eq. (29) can be analytically performed,

$$\mathbb{P}(E_p,\tau) = [3 + \cos(2\vartheta_k)]\tilde{\mathbb{P}}(E_p,\tau), \quad (32)$$

where $\tilde{\mathbb{P}}(E_p,\tau)$ is independent of Λ, ϑ_k, and m. Any measurement of the relative streaking spectrum (that is, of relative photoionization probabilities) will therefore depend on neither the helicity Λ nor the opening angle ϑ_k and the TAM projection m of the X wave pulse. However, measurements of absolute spectra would restore a dependence on the opening angle.

Let us remark that Eq. (31) has a more complex dependence on ϑ_k if the photoelectrons are not observed along the polarization direction of the NIR field. For infinite targets, however, the effect of the TAM projection on the photoionization process is always integrated out. Therefore, the interesting question remains how the streaking spectra depend on the X wave parameters for targets of finite size that are localized around some impact parameter.

IV. CONCLUSION

We investigated theoretically the streaking process where the ionizing pulse is an attosecond X wave carrying orbital angular momentum and the streaking field is a strong NIR plane-wave laser pulse. Emphasis was placed upon the influence of the characteristic opening angle as well as the total angular momentum of the ionizing pulse on the streaking process.

We discovered that the streaking spectra from single-atom targets show a strong dependence on the opening angle of the X wave and the impact parameter of the target relative to the beam axis. Both parameters determine the X wave pulse structure that the atom experiences and therefore the timing of photoelectron emission into the NIR field. For infinitely extended clouds of atoms, we found that the (relative) streaking spectra observed in the polarization direction of the NIR field do not depend on the opening angle or total angular momentum of the X wave.

Recent experimental advances in the creation of ultrashort twisted pulses [24,25] as well as the localization of targets [41] suggest that streaking measurements with small atomic clouds might be possible in the near future. Regarding this, it is an important future task to analyze the influence of a finite

target size on the streaking spectra in the setup discussed here. In addition, more complex atomic or molecular targets may be investigated within the formalism used here. For such targets, due to more ionization channels, the effect of the total angular momentum of the twisted pulse is expected to be more pronounced than for the target considered in this work.

The work presented here opens avenues for more complex two-color experiments involving ultrashort pulses that carry orbital angular momentum. For example, the excitation by an attosecond X wave and subsequent ionization by a strong NIR pulse might provide insight into the dynamics of excited states that differ from those excited by plane-wave pulses due to modified selection rules for localized targets [20]. This promises rich applications in both atomic and molecular physics.

ACKNOWLEDGMENT

The work reported in this paper was supported by the Priority Programme 1840 "Quantum Dynamics in Tailored Intense Fields" (QUTIF) of the German Research Foundation (DFG) under Contract No. FR 1251/17-1.

[1] F. Calegari, G. Sansone, S. Stagira, C. Vozzi, and M. Nisoli, J. Phys. B **49**, 062001 (2016).
[2] P. B. Corkum and F. Krausz, Nat. Phys. **3**, 381 (2007).
[3] S. R. Leone, C. W. McCurdy, J. Burgdörfer, L. S. Cederbaum, Z. Chang, N. Dudovich, J. Feist, C. H. Greene, M. Ivanov, R. Kienberger, U. Keller, M. F. Kling, Z.-H. Loh, T. Pfeifer, A. N. Pfeiffer, R. Santra, K. Schafer, A. Stolow, U. Thumm, and M. J. J. Vrakking, Nat. Photon. **8**, 162 (2014).
[4] M. Schultze *et al.*, Science **328**, 1658 (2010).
[5] M. Drescher, M. Hentschel, R. Kienberger, M. Uiberacker, V. Yakovlev, A. Scrinzi, T. Westerwalbesloh, U. Kleineberg, U. Heinzmann, and F. Krausz, Nature (London) **419**, 803 (2002).
[6] L. Belshaw, F. Calegari, M. J. Duffy, A. Trabattoni, L. Poletto, M. Nisoli, and J. B. Greenwood, J. Phys. Chem. Lett. **3**, 3751 (2012).
[7] F. Calegari, D. Ayuso, A. Trabattoni, L. Belshaw, S. De Camillis, S. Anumula, F. Frassetto, L. Poletto, A. Palacios, P. Decleva, J. B. Greenwood, F. Martín, and M. Nisoli, Science **346**, 336 (2014).
[8] C. Lemell, S. Neppl, G. Wachter, K. Tokesi, R. Ernstorfer, P. Feulner, R. Kienberger, and J. Burgdörfer, Phys. Rev. B **91**, 241101 (2015).
[9] P. Antoine, A. L'Huillier, and M. Lewenstein, Phys. Rev. Lett. **77**, 1234 (1996).
[10] F. Quéré, Y. Mairesse, and J. Itatani, J. Mod. Opt. **52**, 339 (2005).
[11] F. Quéré, J. Itatani, G. L. Yudin, and P. B. Corkum, Phys. Rev. Lett. **90**, 073902 (2003).
[12] J. Itatani, F. Quéré, G. L. Yudin, M. Y. Ivanov, F. Krausz, and P. B. Corkum, Phys. Rev. Lett. **88**, 173903 (2002).
[13] Y. Mairesse and F. Quéré, Phys. Rev. A **71**, 011401 (2005).
[14] N. R. Heckenberg, R. McDuff, C. P. Smith, and A. G. White, Opt. Lett. **17**, 221 (1992).
[15] M. Beijersbergen, R. Coerwinkel, M. Kristensen, and J. Woerdman, Opt. Commun. **112**, 321 (1994).
[16] J. Arlt and K. Dholakia, Opt. Commun. **177**, 297 (2000).
[17] M. Padgett and R. Bowman, Nat. Photon. **5**, 343 (2011).
[18] H. He, M. E. J. Friese, N. R. Heckenberg, and H. Rubinsztein-Dunlop, Phys. Rev. Lett. **75**, 826 (1995).
[19] O. Matula, A. G. Hayrapetyan, V. G. Serbo, A. Surzhykov, and S. Fritzsche, J. Phys. B **46**, 205002 (2013).
[20] H. M. Scholz-Marggraf, S. Fritzsche, V. G. Serbo, A. Afanasev, and A. Surzhykov, Phys. Rev. A **90**, 013425 (2014).
[21] A. Picón, J. Mompart, J. R. V. de Aldana, L. Plaja, G. F. Calvo, and L. Roso, Opt. Express **18**, 3660 (2010).
[22] M. Zürch, C. Kern, P. Hansinger, A. Dreischuh, and C. Spielmann, Nat. Phys. **8**, 743 (2012).
[23] C. Hernández-García, A. Picón, J. San Román, and L. Plaja, Phys. Rev. Lett. **111**, 083602 (2013).
[24] G. Gariepy, J. Leach, K. T. Kim, T. J. Hammond, E. Frumker, R. W. Boyd, and P. B. Corkum, Phys. Rev. Lett. **113**, 153901 (2014).
[25] L. Rego, J. S. Román, A. Picón, L. Plaja, and C. Hernández-García, Phys. Rev. Lett. **117**, 163202 (2016).
[26] E. Hemsing, A. Knyazik, M. Dunning, D. Xiang, A. Marinelli, C. Hast, and J. B. Rosenzweig, Nat. Phys. **9**, 549 (2013).
[27] P. R. Ribič, D. Gauthier, and G. De Ninno, Phys. Rev. Lett. **112**, 203602 (2014).
[28] C. Conti, S. Trillo, P. Di Trapani, G. Valiulis, A. Piskarskas, O. Jedrkiewicz, and J. Trull, Phys. Rev. Lett. **90**, 170406 (2003).
[29] A. Ciattoni and C. Conti, J. Opt. Soc. Am. B **24**, 2195 (2007).
[30] C. Conti and S. Trillo, Phys. Rev. Lett. **92**, 120404 (2004).
[31] J.-y Lu and S. He, Opt. Commun. **161**, 187 (1999).
[32] M. Ornigotti, C. Conti, and A. Szameit, Phys. Rev. Lett. **115**, 100401 (2015).
[33] M. Ornigotti, C. Conti, and A. Szameit, Phys. Rev. A **92**, 043801 (2015).
[34] M. Ornigotti, C. Conti, and A. Szameit, J. Opt. **18**, 075605 (2016).
[35] R. A. Müller, D. Seipt, R. Beerwerth, M. Ornigotti, A. Szameit, S. Fritzsche, and A. Surzhykov, Phys. Rev. A **94**, 041402 (2016).
[36] D. Bauer, D. B. Milošević, and W. Becker, Phys. Rev. A **72**, 023415 (2005).
[37] D. Seipt, R. A. Müller, A. Surzhykov, and S. Fritzsche, Phys. Rev. A **94**, 053420 (2016).
[38] *Localized Waves*, edited by H. E. Hernández-Figueroa, M. Zamboni-Rached, and E. Recami (Wiley, New York, 2008).
[39] A. K. Kazansky, A. V. Grigorieva, and N. M. Kabachnik, Phys. Rev. A **85**, 053409 (2012).
[40] G. N. Watson, *A Treatise on the Theory of Bessel Functions*, 1st ed. (Cambridge University Press, Cambridge, 1922).
[41] C. T. Schmiegelow, J. Schulz, H. Kaufmann, T. Ruster, U. G. Poschinger, and F. Schmidt-Kaler, Nat. Commun. **7**, 12998 (2016).